ARTICLE   OPEN

Check for updates

Climate responses in China to domestic and foreign aerosol changes due to clean air actions during 2013–2019

Jiyuan Gao [1], Yang Yang [1 ✉], Hailong Wang [2], Pinya Wang[1], Baojie Li[1], Jiandong Li [1], Jiangfeng Wei[3], Meng Gao [4] and Hong Liao[1]

In recent years, to improve air quality, significant efforts have been made to reduce regional aerosols including China, Europe and North America, which have potential impacts on climate. In this study, fast and slow climate responses in China to changes in domestic and foreign anthropogenic emissions of aerosols and precursors from 2013 to 2019 are investigated using the Community Earth System Model version 1 (CESM1). Aerosol emissions changes, especially reductions in China, North America and Europe, during 2013–2019 resulted in surface air temperature increases across the Northern Hemisphere. Global aerosol changes induce a regional warming of 0.2 °C in China, equally contributed by domestic and foreign emissions changes. China's domestic emission reductions lead to a regional average temperature rise of 0.1°C, primarily driven by rapid atmospheric adjustments over eastern China. Foreign aerosol changes, particularly reductions in North America and Europe, also contributed to a 0.1°C warming in China through slow oceanic processes. This warming in China induced by foreign aerosol changes is due to a teleconnection between the aerosol-induced anomalous regional warming in Eastern U.S.-North Atlantic Ocean-Europe and the downstream East Asian climate through anomalous wave trains propagation. The comparable influence of domestic and foreign aerosol changes on climate in China underscores the importance of international collaboration in climate mitigation endeavors.

INTRODUCTION

Aerosol, as one of the most critical pollutants in the atmosphere, is harmful to environment, human health, and ecosystems[1], and it is also considered as a short-lived climate forcer that has an impact on global and regional climate through interacting with radiation and clouds[2]. It is estimated that the global mean aerosol effective radiative forcing (ERF) at the top of the atmosphere (TOA) in 2019 relative to 1750 is -1.1 (-1.7 to -0.4) W m^{-2}, with -0.22 (-0.47 to 0.04) W m^{-2} contributed from aerosol–radiation interactions and -0.84 (-1.45 to -0.25) W m^{-2} attributed to aerosol–cloud interactions. It leads to the global surface air temperature changed by -0.13 (-0.28 to -0.01) °C from aerosol-radiation interactions and -0.38 (-0.77 to -0.12) °C from aerosol-cloud interactions[3].

Aerosols have been changing considerably throughout the globe. In the 1980s, clean air actions were implemented in North America and Europe and emissions of aerosols and their precursors have decreased since then[4,5]. As a consequence, near-surface aerosol concentrations and aerosol optical depth (AOD) over North America and Europe have declined during the past decades reported from long-term ground observations, satellite retrievals and model simulations[6–14]. Unlike developed countries in Europe and America, other developing regions such as South Asia continued to maintain high levels of emissions, with the aerosol levels still showing a significant increase[5,15]. In China, Air Pollution Prevention and Control Action Plan was promulgated in 2013 to deal with the serious air pollution issues. Subsequently, the emissions of aerosols and precursors have been reduced and aerosol concentrations have declined over China[16–18]. Ground observations indicated that the near-surface PM$_{2.5}$ (particulate

matter with diameter less than 2.5 μm) concentrations in China decreased by about 33.3% during 2013–2017[19].

Changes in aerosol, as an important climate forcer, come with local and regional climate impacts. During the period 1980–2010, aerosol emissions reductions in the U.S. caused changes in aerosol direct radiative forcing (DRF) by 0.8 W m^{-2} and indirect radiative forcing (IRF) by 1.0 W m^{-2} over eastern U.S., resulting in a 0.35 °C warming in the U.S.[20,21]. It has also been estimated that aerosol decreases over Europe lead to a DRF change of 1.26 W m^{-2} between the 1980s and 1990s[22]. Based on the chemical transport model GEOS-Chem, Dang and Liao[23] found a regional mean change in DRF of 1.18 W m^{-2} in 2017 relative to 2012 resulting from the reduction in aerosols over eastern China. Zheng et al.[16] reported that the decreased aerosol emissions in China during 2006–2017 exerted an anomalous ERF of 0.48 ± 0.11 W m^{-2} and a surface air warming of 0.12 ± 0.02 °C in East Asia. Gao et al.[18] also estimated a warming of 0.09 ± 0.10 °C in eastern China contributed by decreases in domestic aerosols related to clean air policies during 2013–2017.

Aerosols affect climate not only over regions where aerosols are emitted, but also over remote areas. Cowan & Cai[24] attributed the decreased Asian monsoon rainfall to strengthened northerly flows related to non-Asian aerosols. Wang et al.[25] found an anomalous cooling in summer over East Asia partly due to eastward cold advections in the midlatitudes of the Northern Hemisphere caused by European aerosol forcing based on global aerosol–climate model simulations. Mahmood & Li[26] demonstrated that South Asian black carbon (BC) aerosol could change the regional pattern of East Asian summer monsoon rainfall in

[1]Joint International Research Laboratory of Climate and Environment Change (ILCEC), Jiangsu Key Laboratory of Atmospheric Environment Monitoring and Pollution Control, Jiangsu Collaborative Innovation Center of Atmospheric Environment and Equipment Technology, School of Environmental Science and Engineering, Nanjing University of Information Science and Technology, Nanjing, Jiangsu, China. [2]Atmospheric Sciences and Global Change Division, Pacific Northwest National Laboratory, Richland, WA, USA. [3]School of Atmospheric Sciences, Nanjing University of Information Science and Technology, Nanjing, Jiangsu, China. [4]Department of Geography, State Key Laboratory of Environmental and Biological Analysis, Hong Kong Baptist University, Hong Kong SAR, China. ✉email: yang.yang@nuist.edu.cn

China related to a propagating wave train along the Asian upper tropospheric jet induced by an increase in South Asian BC. Liu et al.[27] also found that the growth in South Asian aerosols during 2013–2017 increased surface air temperature over central-eastern China and enhanced East Asian summer monsoon strength through changing large-scale atmospheric circulations. Wilcox et al.[28] showed significant climate responses across the mid-latitude to Asian anthropogenic aerosols related to the aerosol-generated Rossby waves. Fahrenbach & Bollasina[29] investigated climate impacts of COVID-19-related Asian aerosol emission reductions and discovered a Hemispheric-wide response because of stationary Rossby wave trains from East Asia. In addition, Westervelt et al.[30], Acosta Navarro et al.[31] and Kasoar et al.[32] all studied climate responses to aerosols from individual source regions in the Northern Hemisphere and reported a wide range of temperature responses across the hemisphere.

Climate responses to external forcers including anthropogenic aerosols can be decomposed into fast and slow climate responses[33–35]. Fast climate responses refer to changes in climate variables associated with the rapid atmospheric adjustments before significant changes in surface temperature, which occur on the timescale from days to months. Slow climate responses occur on a longer timescale of years, which refer to changes in climate variables associated with slow oceanic processes. Many previous studies have investigated fast and slow climate responses, especially precipitation response, to anthropogenic aerosols[34–38]. Kvalevåg et al.[36] suggested that the fast response in precipitation is strongly correlated with radiative forcing associated with atmospheric absorption, while the slow response mostly depends on radiative forcing at TOA. Samset et al.[34] also found that the response in precipitation over a number of land regions is more dominated by rapid adjustments than temperature-driven slow processes. Zhang et al.[35] analyzed the fast and slow responses of precipitation to BC and sulfate perturbations and found a decrease in global-mean precipitation attributed to fast responses to BC perturbation and slow responses to sulfate perturbation. A few studies also discussed fast and slow responses in monsoon system to aerosols[33,39]. For example, Wang et al.[39] found that East Asian summer monsoon was weakened due to a decreased land-sea temperature contrast in the fast response to sulfate forcing, and this effect was strengthened by the subsequent tropospheric thermodynamic and dynamic structure changes due to the slow response.

With the fast climate responses considered alone, Gao et al.[18] suggested that domestic reductions in aerosols and precursor emissions related to local clean air actions induced less significant warming over eastern China, in which the slow oceanic process was not included. In this study, inspired by Gao et al.[18], we aim to quantify climate responses in China to changes in both domestic and foreign anthropogenic emissions of aerosols and their precursors during 2013–2019 using the Community Earth System Model version 1 (CESM1) and decompose the climate responses to the fast and slow components to improve the understanding of the physics underlying the responses.

RESULTS

Changes in anthropogenic aerosols from 2013 to 2019

Since 2013 when clean air actions were taken in China, anthropogenic emissions of aerosols and their precursors showed great reductions over China (Supplementary Fig. 1). Sulfur dioxide, BC, and organic carbon emissions decreased by −34.2, −0.8, and −0.58 Tg year^{-1}, respectively, over China during 2013–2019. Although the emission reductions in Europe and North America experienced an unexpected slowdown in the past decade[11,40], reductions in aerosols and precursor emissions can also be observed in these two regions.

Drastic declines in near-surface $PM_{2.5}$ concentrations (sum of sulfate, BC, POM, SOA, dust×0.1, and sea-salt×0.25 following Turnock et al.[41]) are observed over eastern China in both model results and observations (Fig. 1). The model and observations also indicate a significant reduction in near-surface $PM_{2.5}$ concentrations over eastern U.S. and Europe, but the reduction in Europe and eastern U.S. is not as substantial as in China. The simulated and satellite AOD also show decreases in China, eastern U.S., and Europe (Supplementary Fig. 2). Please see the detailed model evaluation in the Methods section.

Climate responses to anthropogenic aerosol changes

As a short-lived climate forcer, aerosols affect climate by altering the earth's radiation budget through interacting with radiation and clouds. The implementation of clean air actions in China resulted in notable reductions in anthropogenic aerosols and precursor emissions, which led to a decrease in near-surface $PM_{2.5}$ concentrations, as illustrated above. The reductions in aerosols further caused an anomalous aerosol ERF of 0.64 W m^{-2} at TOA, averaged over China in 2019 relative to 2013, with the largest ERF anomaly exceeding 2 W m^{-2} in southern China (Fig. 2a). Concurrently, the emission reductions policies implemented in Europe and North America induced an anomalous ERF of 0.48 and 0.45 W m^{-2}, respectively, over these two local regions. Note that, in $PM_{2.5}$, both absorbing aerosol (i.e., BC) and scattering aerosols (i.e., sulfate, POM and SOA) decreased over China, Europe and North America. The positive ERF anomaly at TOA indicates that the climate impacts of aerosol changes during 2013–2019 are dominated by the scattering aerosols.

The positive ERF anomalies induced by aerosol reductions led to an increase in surface air temperatures in China, North America and Europe during 2013–2019. Regional averages of surface air temperatures in China, North America and Europe increased by 0.20, 0.15 and 0.14 °C, respectively (Fig. 3). Due to the emission reductions mainly occurring in the Northern Hemisphere, temperature increases in the Northern Hemisphere are much more pronounced than those in the Southern Hemisphere. Moreover, warming is not only limited to areas of emission reductions. The aerosol reduction-induced warming spreads across the Northern Hemisphere, including land and ocean regions, which has been reported in previous studies[29,30,32]. In addition, a faster warming in the Arctic than other regions related to Arctic amplification is also observed, which has been attributed to a combination of positive feedback mechanisms in the Arctic climate system[42–47].

The warming induced by aerosol emissions reductions in the Northern Hemisphere influenced the hemispheric temperature contrasts, leading to a northward shift of the intertropical convergence zone occurred towards the warmer hemisphere[48,49], as also depicted in Fig. 3. However, the precipitation changes over most of the continental regions are statistically insignificant, likely related to the small perturbation of aerosols during 2013–2019, especially the solar-absorbing particles, compared to the internal variability.

Responses in climate of China to domestic and foreign aerosol changes

In this section, climate responses over China to changes in global, domestic and foreign anthropogenic emissions of aerosols and precursors, and contributions from fast and slow processes are quantified, as shown in Fig. 4. A regional warming of 0.2 °C over China (Fig. 4a) is equally attributed to domestic (Fig. 4b) and foreign (Fig. 4c) emission reductions, i.e., each contributing to 0.1 °C of the increase in temperature, but the spatial warming patterns are different between the domestic and foreign contributions. Due to the reductions in China's domestic emissions, aerosol decrease-induced warming (Fig. 4b) is contributed by both rapid atmospheric adjustments (Fig. 4e) and slow oceanic
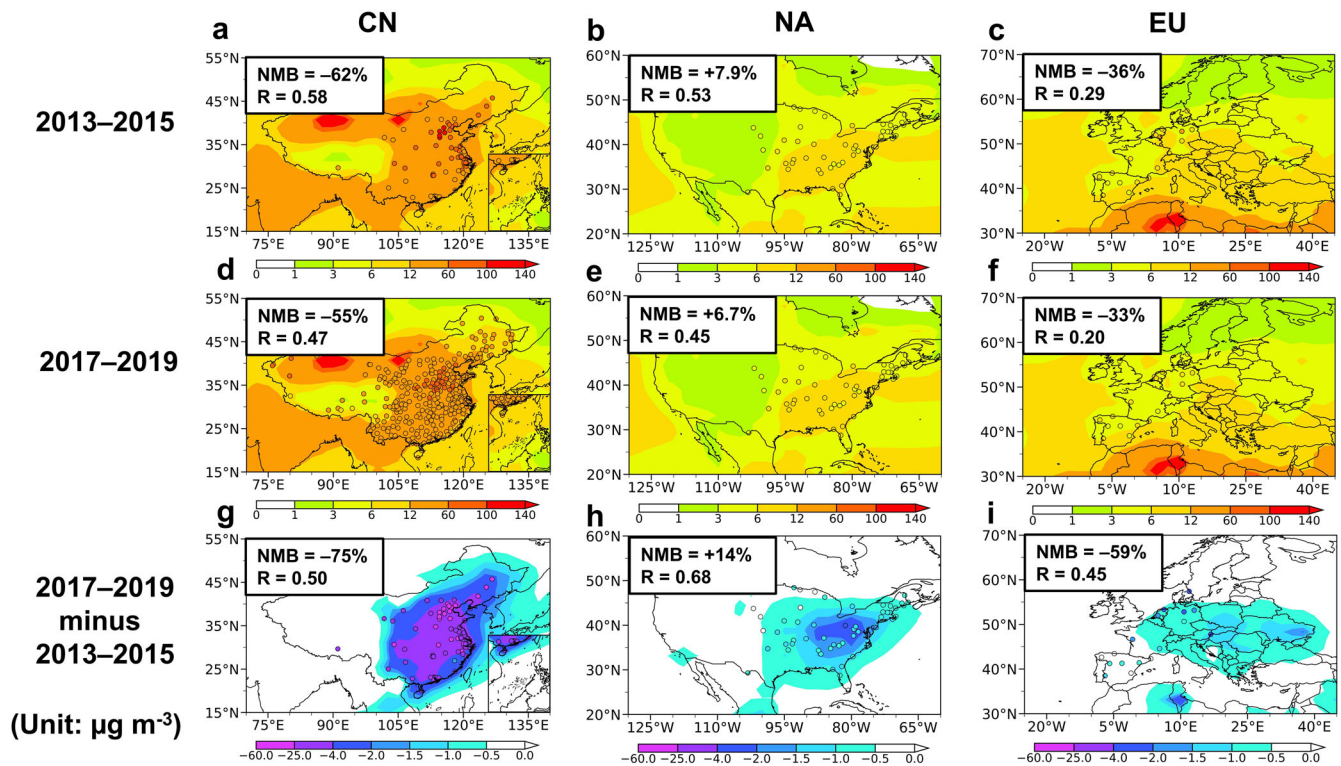
Fig. 1 Comparisons of near-surface PM$_{2.5}$ concentrations between observations and simulations. Spatial distributions of observed (circles) and simulated (shades) annual mean near-surface PM$_{2.5}$ concentrations (sum of sulfate, BC, POM, SOA, dust×0.1, and sea-salt×0.25) during 2013–2015 (**a–c**), 2017–2019 (**d–f**), and their differences (**g–i**, 2017–2019 minus 2013–2015) over China (**a, d** and **g**, CN), North America (**b, e** and **h**, NA), and Europe (**c, f** and **i**, EU). Normalized mean bias (NMB) and correlation coefficient (R) between observation and simulation are shown at the upper-left corner of each panel. *NMB = 100% × ∑ (Model$_i$ − Observation$_i$)/ ∑ Observation$_i$, where Model$_i$ and Observation$_i$* are the modeled and observed values at site *i*, respectively.
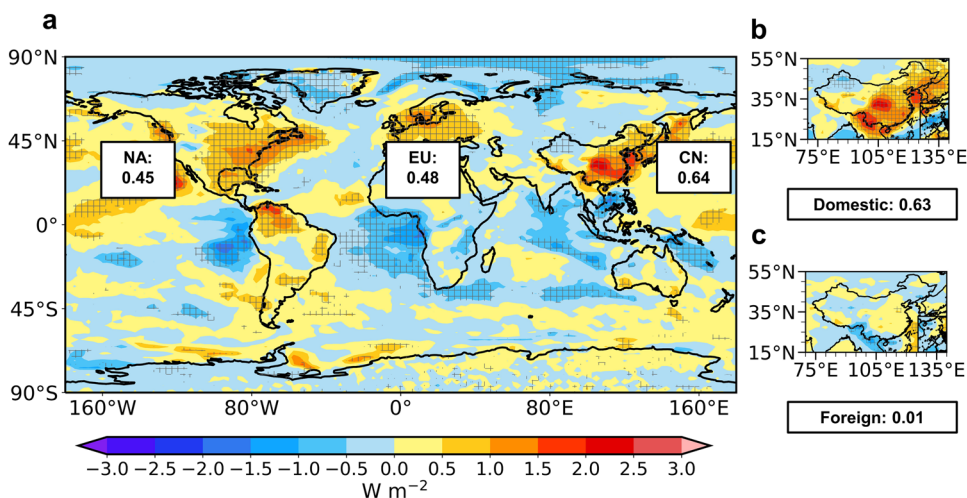

Fig. 2 Changes in effective radiative forcing (ERF) due to changes in anthropogenic emissions of aerosols and precursors. Spatial distributions of changes in annual mean ERF (W m^{-2}) due to changes in (**a**) global, (**b**) China's domestic and (**c**) foreign anthropogenic emissions of aerosols and precursors in 2019 relative to 2013. Changes in ERF are calculated as the differences in net radiative fluxes at the top of the atmosphere. The shaded areas indicate results are statistically significant at the 90% confidence level. Regional averages of the changes over China (CN), North America (NA) and Europe (EU) are noted near these regions.

processes (Fig. 4h). Over eastern China, the fast climate response (Fig. 4e) dominates the warming caused by domestic aerosol reductions, in accordance with the positive ERF anomaly over this region (Fig. 2b). Although temperature increases are also located in western China due to the slow climate response (Fig. 4h), they are statistically insignificant and may be related to the internal variability of the model.

It is intriguing to note that foreign aerosol changes significantly enhance the warming over China during 2013–2019 (Fig. 4c). Over eastern China, slow climate responses control the local warming from foreign contributions, with the maximum warming approaching 0.3 °C (Fig. 4i). Besides, the increasing aerosols during 2013–2019 in South Asia and Southeast Asia enhanced the transboundary aerosol transport into China (Supplementary
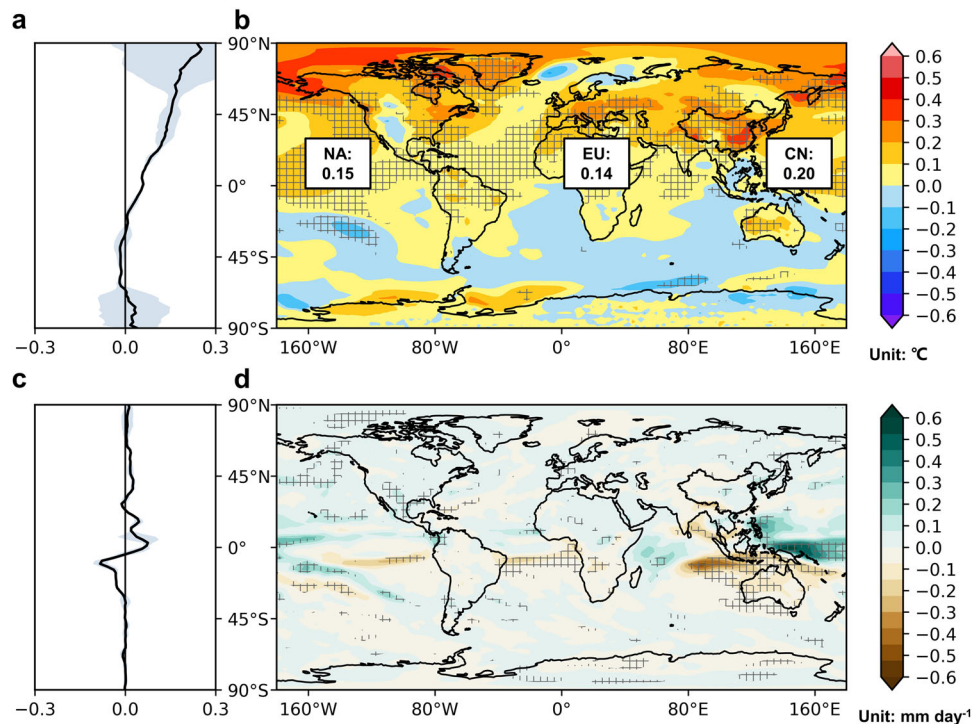
Fig. 3 Changes in surface air temperature and precipitation rate due to changes in anthropogenic emissions of aerosols and precursors. Zonal-mean (**a** and **c**) and spatial distributions of changes (**b** and **d**) in annual mean surface air temperature (°C, **a** and **b**) and precipitation rate (mm day^{-1}, **c** and **d**) due to changes in global anthropogenic emissions of aerosols and precursors from 2013 to 2019. The shaded areas indicate results are statistically significant at the 90% confidence level. Regional averages of the annual mean surface air temperature changes over China (CN), North America (NA) and Europe (EU) are noted in the top panels.

Fig. 3), which causes a cooling over southern China through rapid atmospheric adjustments from the foreign contribution (Fig. 4f). It can be confirmed by the atmosphere-only simulation with emissions in South Asia and Southeast Asia alone changing from 2013 to 2019 (Supplementary Fig. 4). However, the insignificant ERF anomaly contributed by changes in foreign emissions (0.01 W m^{-2}, Fig. 2c) cannot explain the overall warming in eastern China from foreign contributions. With changes in anthropogenic emissions of aerosols and precursors in North America and Europe alone, a 0.1 °C regional warming is also presented in China (Supplementary Fig. 5), which equals to that caused by changes in all foreign emissions. Also, the contribution of warming from emission changes over North America and Europe is mainly through slow oceanic processes (Supplementary Fig. 5c). It suggests that the aerosol reductions in the North America and Europe are the primary contributor to the foreign emission-induced warming in China during 2013–2019. This finding is consistent with previous studies[21,30–32] that a perturbation in aerosol loading in the North America or Europe can exert a significant impact on air temperature in China.

The climate in China is also linked to foreign aerosol changes through teleconnections. Many studies have reported that the North Atlantic Oscillation (NAO) had significant downstream influences on East Asian climate, primarily through quasi-stationary wave propagation of upper-tropospheric anomalies along the Asian jet, along with positive temperature anomalies in East Asia during positive NAO phase[50–52]. The changes in foreign aerosols, especially aerosol reductions in the U.S. and Europe, increase the sea surface temperature (SST) over the North Atlantic Ocean (Supplementary Fig. 6), which is also likely to induce an anomalous warming over East Asia through anomalous wave trains propagation as the NAO influence.

Figure 5 shows total, fast and slow responses of 200 hPa eddy stream function and wave activity flux to changes in foreign

anthropogenic emissions of aerosols and precursors, which have been widely used to examine teleconnection mechanisms[53–55]. Two anomalous wave trains are observed in the total responses, associated with anomalous warming in the Eastern U.S., North Atlantic Ocean, and Europe. One anomalous wave train propagates eastward from the Eastern U.S. to Northern China (via Eastern U.S.–North Atlantic Ocean–the Middle East– the Tibet Plateau–Northern China), while the other one originates from North Atlantic Ocean and Northern Europe, propagating through Kazakhstan to Northern China. In this study, positive stream function anomalies, originating from North America, North Atlantic Ocean, and Europe, propagate when the dynamic ocean is enabled (Fig. 5a), exhibiting remarkable similarities with the positive NAO phase[51]. This implies a teleconnection that links the increase in temperature over China to the reduction of aerosols in North America and Europe. The anomalous wave trains in the fast responses show different patterns than those in the total response, but are less statistically significant (Fig. 5b), while the anomalous wave trains in the slow responses are similar to those observed in the total responses (Fig. 5c). The spatial patterns of 500 hPa temperature, 200 hPa geopotential height, and 200 hPa eddy geopotential height exhibit noticeable similarities as the pattern of 200 hPa eddy stream function, characterized by positive anomalies in Eastern U.S., North Atlantic Ocean, Northern Europe, the Middle East, and Northern China (Fig. 6). These suggest that significant warming in Eastern U.S., North Atlantic Ocean and Europe in response to local aerosol emission reductions have significant remote climate influences via teleconnections when dynamic ocean processes are included, leading to a temperature increase in eastern China.

The teleconnection can also be partly supported based on by the maximum covariance analysis (MCA)[53,56,57] between the surface temperature (TS) over North America, the North Atlantic Ocean, and Europe and the 200 hPa geopotential height (GPH)
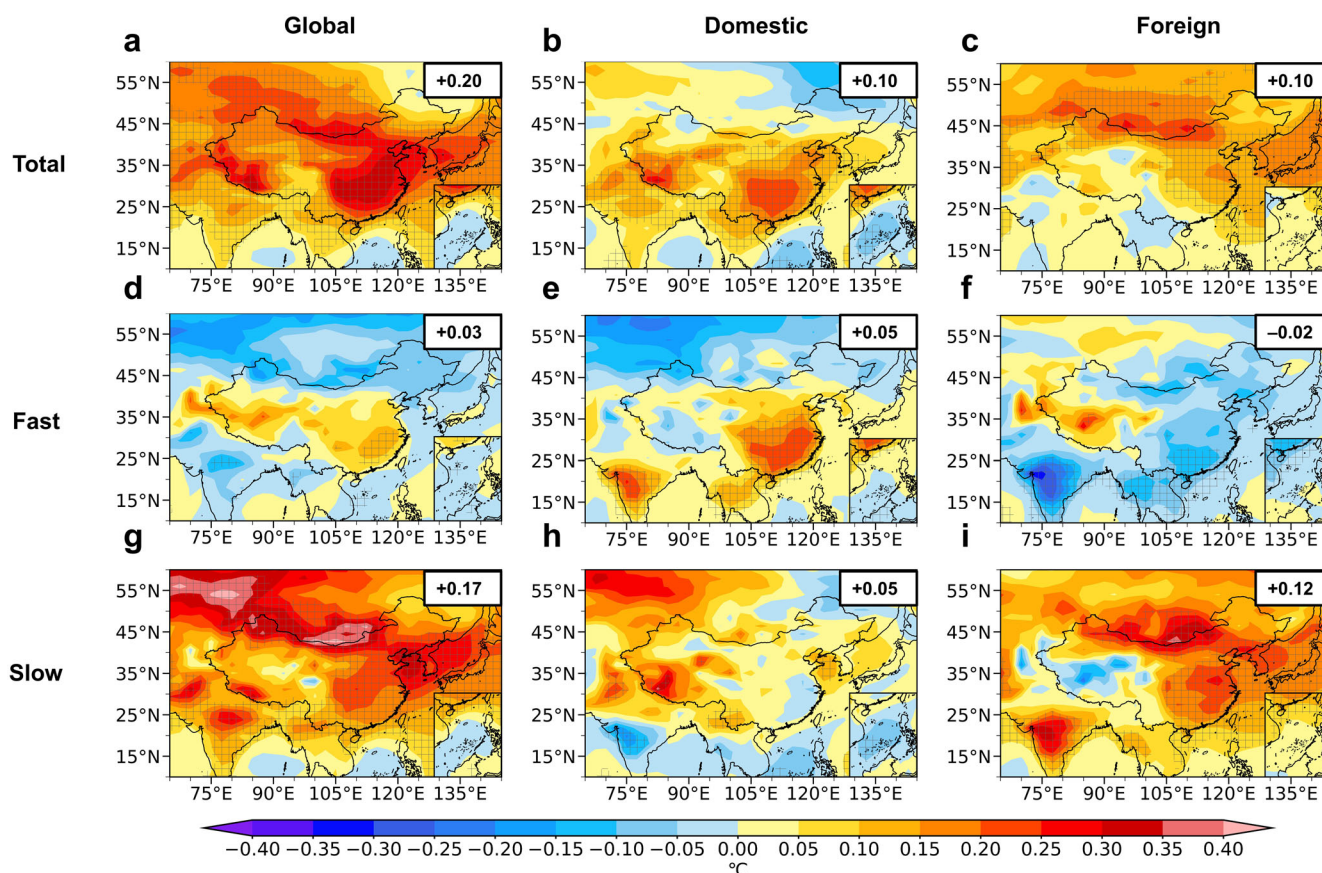
Fig. 4 Changes in surface air temperature due to changes in anthropogenic emissions of aerosols and precursors. Spatial distributions of total (a–c), fast (d–f) and slow (g–i) responses in annual mean surface air temperature (°C) to changes in global (a, d and g), domestic (b, e and h) and foreign (c, f and i) anthropogenic emissions of aerosols and precursors during 2013–2019. The shaded areas indicate results are statistically significant at the 90% confidence level. Regional averages of the responses over China are noted at the upper-right corner of each panel.

during 1970–2020 from EAR-5 reanalysis. Explaining 69.3% of the covariance, the leading MCA mode shows the anomalous high TS over North America, the North Atlantic Ocean, and Europe is accompanied by the anomalous high GPH across Eurasia (Supplementary Fig. 7a), which is in agreement with the CESM1 simulations (Fig. 6b). The associated time series for this mode exhibit a strong correlation, with the correlation coefficient of 0.87 (Supplementary Fig. 7b). Although this mode in observations is more likely related to the global warming caused by the increases in greenhouse gases, the simulated anomalous high GPH induced by changes in foreign emissions between 2013 and 2019 resembling the GPH pattern in observations might contribute to the warming in Northern China.

DISCUSSION

In recent years, Europe and North America have continuously reduced their anthropogenic emissions of aerosols and precursors, and China has also significantly reduced its emissions since the implementation of clean air policies in 2013. Several studies[16,18,23] have reported that clean air actions in China in recent years exerted a local warming, but few of them considered the effects of simultaneous aerosol changes in foreign regions outside China. Additionally, both fast and slow processes can lead to climate change through different mechanisms, but most previous studies did not separate the two processes. This study quantifies the climate responses in China to changes in domestic and foreign emissions of aerosols and precursors during 2013–2019 and distinguishes the fast and slow climate responses using CESM1.

Anthropogenic aerosol concentrations have significantly decreased in China, North America, and Europe during 2013–2019, which further led to increases in surface air temperature across the Northern Hemisphere. The global aerosol changes induce a regional warming by 0.2 °C over China during 2013–2019, which on average is equally contributed by China's domestic and foreign emission changes. Over eastern China where warming is the most significant, the domestic aerosol-induced warming is primarily due to fast climate responses (i.e., rapid atmospheric adjustments). Foreign aerosol changes, especially aerosol reductions in North America and Europe, contributed to an average warming of 0.1 °C in China mainly through slow climate responses (i.e., slow oceanic processes). The foreign aerosol-induced warming is related to anomalous wave train propagation in the Northern Hemisphere associated with anomalous warming in the Eastern U.S., North Atlantic Ocean, and Europe. The comparable magnitude of the influence of domestic and foreign aerosol changes on surface air temperature in China during 2013–2019 highlights the critical role of foreign aerosols in regulating climate in China, which also emphasizes the importance of cooperation and governance between countries in global climate mitigation.

There are several limitations and uncertainties in our study. Firstly, CESM1 significantly underestimates PM$_{2.5}$ concentrations in China and Europe. This underestimation may result from a few factors, including but not limited to uncertainties in new particle formation, strong aerosol wet removal, coarse model resolution, and uncertainties in anthropogenic emissions of aerosols and precursor gases[58–60]. Consequently, the low bias in estimated
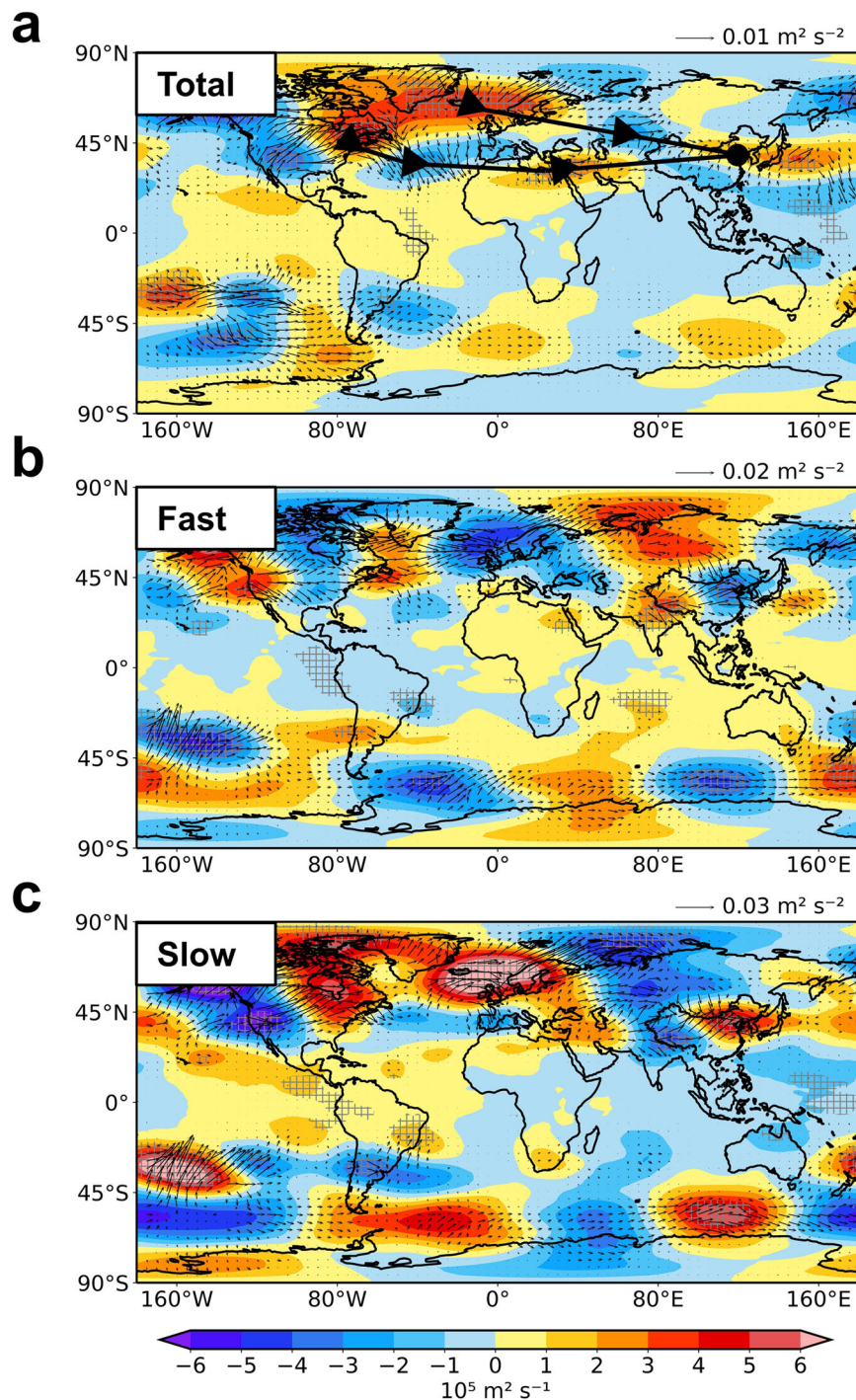
Fig. 5 Changes in 200 hPa eddy stream function and wave activity flux due to changes in foreign anthropogenic emissions of aerosols and precursors. Spatial distributions of (**a**) total, (**b**) fast and (**c**) slow responses in 200 hPa eddy stream function (10^5 m^2 s^{-1}, shades) and wave activity flux (m^2 s^{-2}, vectors) to changes in foreign anthropogenic emissions of aerosols and precursors. The shaded areas indicate results are statistically significant at the 90% confidence level. The stream function and wave activity flux are calculated according to Takaya & Nakamura[78]. The non-zonal/eddy anomalies are obtained by removing the zonal averages in each latitude[53]. Anomalous wave train propagation is shown in black arrows in the top panel.

aerosol could lead to an underestimation of the simulated climate responses. However, the climate responses in China to domestic or foreign emission perturbation may not be linear and CESM1 is more sensitive to anthropogenic forcings than many other climate models[3,61] related to its strong aerosol-cloud interactions[62]. Therefore, the more accurate climate responses to the aerosol

changes need further simulations with a correct AOD and concentration perturbation in further studies with more models[63]. Secondly, nitrate and ammonium, two major components of aerosols, are not explicitly treated in this model version, of which changes must have impacted the climate[59,64]. They need to be considered in future studies. Thirdly, 150-year fully-coupled
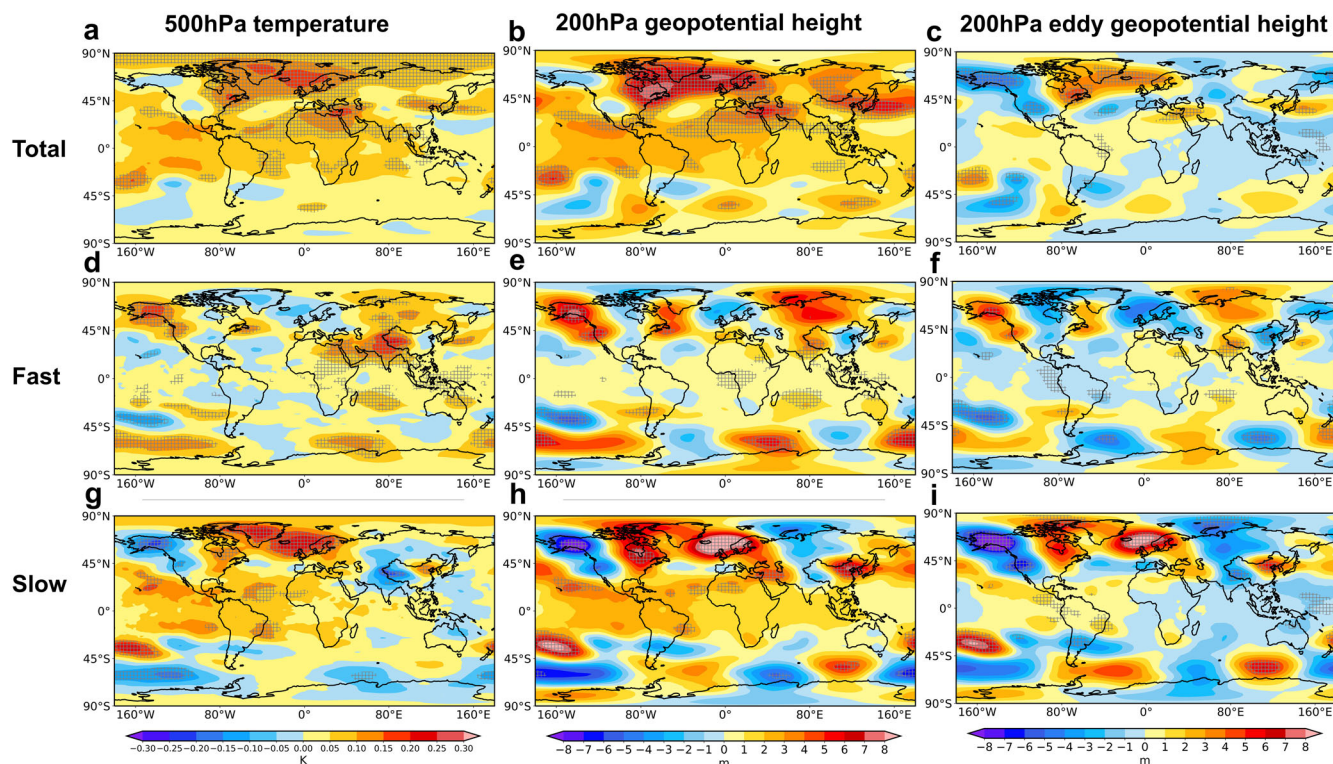
Fig. 6 Changes in 500 hPa temperature, 200 hPa geopotential height and 200 hPa eddy geopotential height due to changes in foreign anthropogenic emissions of aerosols and precursors. Spatial distributions of total (**a**–**c**), fast (**d**–**f**) and slow (**g**–**i**) responses in 500 hPa temperature (K, **a**, **d** and **g**), 200 hPa geopotential height (m, **b**, **e** and **h**) and 200 hPa eddy geopotential height (m, **c**, **f** and **i**) to changes in foreign (non-China) anthropogenic emissions of aerosols and precursors. The shaded areas indicate results are statistically significant at the 90% confidence level.

Table 1.	Experimental design.		
Experiments	Anthropogenic emissions		Model configuration
	China	Rest of the world	
ALL2013	2013	2013	Fully-coupled
CHN2019	2019	2013	Fully-coupled
ALL2019	2019	2019	Fully-coupled
NAEU2019	2013	NA + EU: 2019; Other: 2013	Fully-coupled
ALL2013_FAST	2013	2013	Atmosphere-only
CHN2019_FAST	2019	2013	Atmosphere-only
ALL2019_FAST	2019	2019	Atmosphere-only
NAEU2019_FAST	2013	NA + EU: 2019; Other: 2013	Atmosphere-only
SASEA2019_FAST	2013	SA + SEA: 2019; Other: 2013	Atmosphere-only

The sea surface temperature (SST) and sea ice concentration (SIC) data in the atmosphere-only simulations are derived from the output from the fully coupled experiment ALL2013. NA, EU, SA and SEA represent North America, Europe, South Asia and Southeast Asia, respectively.

equilibrium simulations were conducted in our study, while equilibration with the deep ocean can take thousands of years. Longer simulations may lead to more convincing results. Finally, our results rely on simulations using one single model, and future studies are warranted to employ multi-model ensemble simulations to reduce a potential model dependency.

METHODS

Observational data and meteorological reanalysis
Ground-based observational data of $PM_{2.5}$ concentrations in China, U.S. and Europe are derived from China National Environmental Monitoring Centre (CNEMC), Interagency Monitoring of Protected Visual Environments (IMPROVE) and European Monitoring and Evaluation Programme (EMEP), respectively. These networks provide daily near-surface air pollutant concentrations. AOD data are also obtained from the Moderate Resolution Imaging Spectroradiometer (MODIS) Deep Blue retrieval[65]. These observational data are applied to evaluate the model performance.

ERA-5[66], the fifth generation of the European Centre for Medium-Range Weather Forecasts (ECMWF) atmospheric reanalysis, is a comprehensive dataset with spatial resolution of 0.25 degrees. Monthly surface temperature (TS) and geopotential height (GPH) data from 1970 to 2020 are acquired from ERA-5 for the maximum covariance analysis in our study.

Model description and emissions
In this study, we simulate aerosol climate effects using the global earth system model CESM1[67]. CESM is a comprehensive climate model that simulates the earth's system. Its components include the Community Atmosphere Model (CAM) for atmospheric processes, the Community Land Model (CLM) for terrestrial processes, the Parallel Ocean Program (POP) for global ocean dynamics, and the Community Ice Code (CICE) for polar sea ice processes. It can represent various aspects of the earth's environment and interactions within the climate system. The atmospheric component of CESM1 in this study is CAM version 5 (CAM5), which in this study applies a horizontal resolution of 1.9° latitude × 2.5° longitude and 30-level vertical layers. The four-

mode version of the Modal Aerosol Module (MAM4) within CAM5 predicts aerosol species including sulfate (SO_4^{2-}, generated from its precursor sulfur dioxide (SO_2)), BC, primary organic matter (POM), secondary organic aerosol (SOA, generated from a lumped SOA gas precursor (SOAG)), mineral dust, and sea salt in four lognormal modes (i.e., Aitken, accumulation, coarse, and primary carbon modes)[68]. Sulfate aerosol is mainly produced from its precursor SO_2 through gas-phase oxidation and aqueous-phase oxidation in bulk cloud water. The treatment of SOA is to assume fixed mass yields for precursor volatile organic compound, then directly emit this mass as primary aerosol particles. MAM adds one additional step of complexity by simulating a single lumped semi-volatile organics gas-phase species, which is referred to as SOAG in the model. The CAM5 model includes aerosol-radiation interaction in shortwave and longwave bands as well as aerosol-cloud interactions for stratiform clouds[69]. The double-moment formulation of Morrison and Gettelman[70] and Gettelman et al.[71] is employed to handle the microphysical processes of this stratiform cloud. It enables the prediction of both number and mass mixing ratios of cloud droplets and ice crystals, while the number and mass mixing ratios of rain and snow are diagnosed in the model. Rapid Radiative Transfer Model for General circulation models (RRTMG[72]) is configured in the model for radiative transfer calculations. Precipitation is diagnosed by the Morrison-Gettelman cloud microphysics scheme version 1 (MG1[70,71]). A few modifications for improving the aerosol convective transport and wet deposition are added in the model following Wang et al.[73].

The global anthropogenic emissions of aerosols and precursors are from the latest Community Emissions Data System (CEDS) v_2021_04_21[5]. Different from previous CEDS v_2016_07_26, which has large biases in regional emissions[74], anthropogenic aerosols and precursors emissions were updated with country-level emission inventories of China, Europe and North America. It has now considered the substantial emissions reductions in China due to the clean air actions in recent years. Biomass burning emissions of aerosols and precursors are from CMIP6 (the Coupled Model Intercomparison Project Phase 6)[75]. Biogenic emissions are obtained from the Model of Emissions of Gases and Aerosols from Nature version 2.1 (MEGAN v2.1)[76].

Experimental design

This study aims to quantify the impacts of the changes in domestic and foreign anthropogenic aerosols on climate in China from 2013 to 2019 and investigate the mechanisms of fast and slow climate responses. A series of model experiments are performed using CESM1, as showed in Table 1. ALL2013 is a baseline experiment with a fully-coupled model configuration, in which anthropogenic aerosols and precursors emissions are fixed at year 2013 over the entire globe. In CHN2019, anthropogenic emissions of aerosols and precursors over China are fixed at year 2019 but fixed at year 2013 over all other regions. In ALL2019, anthropogenic emissions of aerosols and precursors are fixed at year 2019 over the entire globe. An additional simulation USEU2019 is also performed, in which anthropogenic emissions of aerosols and precursors over North America and Europe are fixed at year 2019 but fixed at year 2013 over all other regions. All these fully-coupled simulations are run for at least 150 years, with the last 90 years being analyzed. For the purpose of minimizing the model noise, three ensemble members are conducted for each fully-coupled simulation by introducing temperature perturbations to the initial atmospheric conditions.

Another group of atmosphere-only experiments driven by prescribed monthly SST and sea ice concentrations derived from ALL2013 are performed. The experiments are run for 100 years, with the last 90 years selected for analysis. The emission setup in the atmosphere-only experiments is identical to that in the corresponding fully-coupled experiments. These atmosphere-only simulations are used to quantify climate responses that are attributable to the fast processes and to estimate changes in ERF imposed by changes in anthropogenic emissions of aerosols and precursors. Note that, to identify the impacts of changes in emissions from South Asia and Southeast Asia through fast processes, one additional atmosphere-only experiment SASEA2019_FAST is also conducted, in which anthropogenic emissions of aerosols and precursors over South Asia and Southeast are fixed at year 2019 but fixed at year 2013 over all other regions.

Total climate responses to emissions changes are illustrated by the differences between each pair of the fully-coupled simulations. Total climate responses to changes in anthropogenic emissions of aerosols and precursors from the entire globe, China, non-China regions, as well as North America and Europe, during 2013–2019 are identified as the differences between ALL2013 and ALL2019, ALL2013 and CHN2019, CHN2019 and ALL2019, and ALL2013 and NAEU2019, respectively. Fast climate responses are calculated as the differences between each pair of the atmosphere-only simulations, while differences between total response and fast response are attributed to slow response.

Model evaluation

The simulated near-surface $PM_{2.5}$ concentrations in China, North America and Europe in years 2013 and 2019 and the changes during this time period are compared with observations in Fig. 1. Note that, to minimize the meteorological influences on the aerosol observations, the observational data are averaged during 2013–2015 and 2017–2019. The use of smoothing for model evaluation has been employed in previous studies[11,12]. The model simulations can capture the observed spatial distribution of annual average near-surface $PM_{2.5}$ concentrations in China and the changes during 2013–2019, with statistically significant correlation coefficients within the range of 0.5–0.6. However, the model considerably underestimates the $PM_{2.5}$ concentrations and their declines by about 50–80% in China. Such biases have been documented in many previous studies[18,60], which can be partly attributed to uncertainties in new particle formation, uncertainties in anthropogenic emissions of aerosols and precursor gases, and coarse model resolution[58,59]. The comparison between the European $PM_{2.5}$ concentrations from the model and observations shows statistically significant correlation coefficients of 0.2–0.5, but still having a severe underestimation by 30%–60% in the annual mean concentrations and the decreases during 2013–2019. The underestimation in Europe was also reported in previous studies[77]. Both the model and observations indicate a significant reduction in near-surface $PM_{2.5}$ concentrations over eastern U.S., and the model exhibits a good performance in reproducing the magnitude of the $PM_{2.5}$ concentrations and changes with bias below 15%.

The model can well reproduce the spatial pattern with substantial decreases in AOD over eastern China and eastern U.S., but still underestimates the magnitude of the decrease in China by 69%, which suggests that climate effects due to aerosol reductions in China are likely underestimated by the model. Note that the 3-year smoothing of the observations cannot fully remove meteorological influences and the comparison here is only for reference. For example, in Europe, both the annual mean $PM_{2.5}$ concentration and AOD are underestimated by 50–60% and the change in $PM_{2.5}$ concentration during 2013–2019 is also underestimated by 60%, but the change in AOD is overestimated. Therefore, we speculate that the influence of aerosol reductions in Europe is likely underestimated in the CESM1 experiments.

DATA AVAILABILITY

CODE AVAILABILITY

REFERENCES

1. Yang, Y. et al. Global source attribution of sulfate concentration and direct and indirect radiative forcing. *Atmos. Chem. Phys.* **17**, 8903–8922 (2017).
2. Li, J. et al. Scattering and absorbing aerosols in the climate system. *Nat. Rev. Earth. Environ.* **3**, 363–379 (2022).
3. IPCC. *Climate Change 2021: The Physical Science Basis* (Cambridge Univ. Press, 2021).
4. Smith, S. J. et al. Anthropogenic sulfur dioxide emissions: 1850–2005. *Atmos. Chem. Phys.* **11**, 1101–1116 (2011).
5. Hoesly, R. M. & Smith, S. J. Informing energy consumption uncertainty: an analysis of energy data revisions. *Environ. Res. Lett.* **13**, 124023 (2018).
6. Streets, D. G., Tsai, N. Y., Akimoto, H. & Oka, K. Sulfur dioxide emissions in Asia in the period 1985–1997. *Atmos. Environ.* **34**, 4413–4424 (2000).
7. de Meij, A., Pozzer, A. & Lelieveld, J. Trend analysis in aerosol optical depths and pollutant emission estimates between 2000 and 2009. *Atmos. Environ.* **51**, 75–85 (2012).
8. Tørseth, K. et al. Introduction to the European Monitoring and Evaluation Programme (EMEP) and observed atmospheric composition change during 1972–2009. *Atmos. Chem. Phys.* **12**, 5447–5481 (2012).
9. Zhang, H., Hu, J., Kleeman, M. & Ying, Q. Source apportionment of sulfate and nitrate particulate matter in the Eastern United States and effectiveness of emission control programs. *Sci. Total Environ.* **490**, 171–181 (2014).
10. Chin, M. et al. Multi-decadal aerosol variations from 1980 to 2009: a perspective from observations and a global model. *Atmos. Chem. Phys.* **14**, 3657–3690 (2014).
11. Yang, Y. et al. Source Apportionments of Aerosols and Their Direct Radiative Forcing and Long-Term Trends Over Continental United States. *Earth's Future* **6**, 793–808 (2018).
12. Yang, Y., Lou, S., Wang, H., Wang, P. & Liao, H. Trends and source apportionment of aerosols in Europe during 1980–2018. *Atmos. Chem. Phys.* **20**, 2579–2590 (2020).
13. Cherian, R. & Quaas, J. Trends in AOD, Clouds, and Cloud Radiative Effects in Satellite Data and CMIP5 and CMIP6 Model Simulations Over Aerosol Source Regions. *Geophys. Res. Lett.* **47**, e2020GL087132 (2020).
14. Mortier, A. et al. Evaluation of climate model aerosol trends with ground-based observations over the last 2 decades – an AeroCom and CMIP6 analysis. *Atmos. Chem. Phys.* **20**, 13355–13378 (2020).
15. Samset, B. H., Lund, M. T., Bollasina, M., Myhre, G. & Wilcox, L. Emerging Asian aerosol patterns. *Nat. Geosci.* **12**, 582–584 (2019).
16. Zheng, Y., Zhang, Q., Tong, D., Davis, S. J. & Caldeira, K. Climate effects of China's efforts to improve its air quality. *Environ. Res. Lett.* **15**, 104052 (2020).
17. Li, H. et al. Constructing a spatiotemporally coherent long-term PM2.5 concentration dataset over China during 1980–2019 using a machine learning approach. *Sci. Total Environ.* **765**, 144263 (2021).
18. Gao, J. et al. Fast climate responses to emission reductions in aerosol and ozone precursors in China during 2013–2017. *Atmos. Chem. Phys.* **22**, 7131–7142 (2022).
19. Huang, J., Pan, X., Guo, X. & Li, G. Health impact of China's Air Pollution Prevention and Control Action Plan: an analysis of national air quality monitoring and mortality data. *Lancet Planet. Health* **2**, e313–e323 (2018).
20. Leibensperger, E. M. et al. Climatic effects of 1950–2050 changes in US anthropogenic aerosols – Part 1: Aerosol trends and radiative forcing. *Atmos. Chem. Phys.* **12**, 3333–3348 (2012).
21. Leibensperger, E. M. et al. Climatic effects of 1950–2050 changes in US anthropogenic aerosols – Part 2: Climate response. *Atmos. Chem. Phys.* **12**, 3349–3362 (2012).
22. Pozzoli, L. et al. Re-analysis of tropospheric sulfate aerosol and ozone for the period 1980–2005 using the aerosol-chemistry-climate model ECHAM5-HAMMOZ. *Atmos. Chem. Phys.* **11**, 9563–9594 (2011).
23. Dang, R. & Liao, H. Radiative Forcing and Health Impact of Aerosols and Ozone in China as the Consequence of Clean Air Actions over 2012–2017. *Geophys. Res. Lett.* **46**, 12511–12519 (2019).
24. Cowan, T. & Cai, W. The impact of Asian and non-Asian anthropogenic aerosols on 20th century Asian summer monsoon. *Geophys. Res. Lett.* **38**, L11703 (2011).
25. Wang, Z., Mu, J., Yang, M. & Yu, X. Reexamining the Mechanisms of East Asian Summer Monsoon Changes in Response to Non–East Asian Anthropogenic Aerosol Forcing. *J. Clim.* **33**, 2929–2944 (2020).
26. Mahmood, R. & Li, S. Remote influence of South Asian black carbon aerosol on East Asian summer climate. *Int. J. Climatol.* **34**, 36–48 (2014).
27. Liu, C. et al. Influence of Spatial Dipole Pattern in Asian Aerosol Changes on East Asian Summer Monsoon. *J. Clim.* **36**, 1575–1585 (2023).
28. Wilcox, L. J. et al. Mechanisms for a remote response to Asian anthropogenic aerosol in boreal winter. *Atmos. Chem. Phys.* **19**, 9081–9095 (2019).
29. Fahrenbach, N. L. S. & Bollasina, M. A. Hemispheric-wide climate response to regional COVID-19-related aerosol emission reductions: the prominent role of atmospheric circulation adjustments. *Atmos. Chem. Phys.* **23**, 877–894 (2023).
30. Westervelt, D. M. et al. Local and remote mean and extreme temperature response to regional aerosol emissions reductions. *Atmos. Chem. Phys.* **20**, 3009–3027 (2020).
31. Acosta Navarro, J. C. et al. Amplification of Arctic warming by past air pollution reductions in Europe. *Nat. Geosci.* **9**, 277–281 (2016).
32. Kasoar, M., Shawki, D. & Voulgarakis, A. Similar spatial patterns of global climate response to aerosols from different regions. *npj Clim. Atmos. Sci.* **1**, 12 (2018).
33. Ganguly, D., Rasch, P. J., Wang, H. & Yoon, J. Fast and slow responses of the South Asian monsoon system to anthropogenic aerosols. *Geophys. Res. Lett.* **39**, L18804 (2012).
34. Samset, B. H. et al. Fast and slow precipitation responses to individual climate forcers: A PDRMIP multimodel study. *Geophys. Res. Lett.* **43**, 2782–2791 (2016).
35. Zhang, S., Stier, P. & Watson-Parris, D. On the contribution of fast and slow responses to precipitation changes caused by aerosol perturbations. *Atmos. Chem. Phys.* **21**, 10179–10197 (2021).
36. Kvalevåg, M. M., Samset, B. H. & Myhre, G. Hydrological sensitivity to greenhouse gases and aerosols in a global climate model. *Geophys. Res. Lett.* **40**, 1432–1438 (2013).
37. Long, S.-M., Xie, S.-P., Zheng, X.-T. & Liu, Q. Fast and Slow Responses to Global Warming: Sea Surface Temperature and Precipitation Patterns. *J. Clim.* **27**, 285–299 (2014).
38. Richardson, T. B., Forster, P. M., Andrews, T. & Parker, D. J. Understanding the Rapid Precipitation Response to CO2 and Aerosol Forcing on a Regional Scale. *J. Clim.* **29**, 583–594 (2016).
39. Wang, Z., Lin, L., Yang, M., Xu, Y. & Li, J. Disentangling fast and slow responses of the East Asian summer monsoon to reflecting and absorbing aerosol forcings. *Atmos. Chem. Phys.* **17**, 11075–11088 (2017).
40. Jiang, Z. et al. Unexpected slowdown of US pollutant emission reduction in the past decade. *Proc. Natl Acad. Sci. USA* **115**, 5099–5104 (2018).
41. Turnock, S. T. et al. Historical and future changes in air pollutants from CMIP6 models. *Atmos. Chem. Phys.* **20**, 14547–14579 (2020).
42. Serreze, M. C. & Barry, R. G. Processes and impacts of Arctic amplification: a research synthesis. *Glob. Planet. Change* **77**, 85–96 (2011).
43. Lee, S., Gong, T., Johnson, N., Feldstein, S. B. & Pollard, D. On the Possible Link between Tropical Convection and the Northern Hemisphere Arctic Surface Air Temperature Change between 1958 and 2001. *J. Clim.* **24**, 4350–4367 (2011).
44. Goosse, H. et al. Quantifying climate feedbacks in polar regions. *Nat. Commun.* **9**, 1919 (2018).
45. Zhang, R., Wang, H., Fu, Q., Rasch, P. J. & Wang, X. Unraveling driving forces explaining significant reduction in satellite-inferred Arctic surface albedo since the 1980s. *Proc. Natl Acad. Sci. USA* **116**, 23947–23953 (2019).
46. Ren, L. et al. Source attribution of Arctic black carbon and sulfate aerosols and associated Arctic surface warming during 1980–2018. *Atmos. Chem. Phys.* **20**, 9067–9085 (2020).
47. Previdi, M., Smith, K. L. & Polvani, L. M. Arctic amplification of climate change: a review of underlying mechanisms. *Environ. Res. Lett.* **16**, 093003 (2021).
48. Hwang, Y.-T., Frierson, D. M. W. & Kang, S. M. Anthropogenic sulfate aerosol and the southward shift of tropical precipitation in the late 20th century. *Geophys. Res. Lett.* **40**, 2845–2850 (2013).
49. Ridley, H. E. et al. Aerosol forcing of the position of the intertropical convergence zone since AD 1550. *Nat. Geosci.* **8**, 195–200 (2015).

50. Jianping, L. & Wang, J. X. L. A new North Atlantic Oscillation index and its variability. *Adv. Atmos. Sci.* **20**, 661–676 (2003).

51. Linderholm, H. W. et al. Interannual teleconnections between the summer North Atlantic Oscillation and the East Asian summer monsoon. *J. Geophys. Res. Atmos.* **116**, D13107 (2011).

52. Watanabe, M. Asian Jet Waveguide and a Downstream Extension of the North Atlantic Oscillation. *J. Clim.* **17**, 4674–4691 (2004).

53. Ding, Q. et al. Tropical forcing of the recent rapid Arctic warming in northeastern Canada and Greenland. *Nature* **509**, 209–212 (2014).

54. Li, J. et al. Winter particulate pollution severity in North China driven by atmospheric teleconnections. *Nat. Geosci.* **15**, 349–355 (2022).

55. Zou, Y., Wang, Y., Xie, Z., Wang, H. & Rasch, P. J. Atmospheric teleconnection processes linking winter air stagnation and haze extremes in China with regional Arctic sea ice decline. *Atmos. Chem. Phys.* **20**, 4999–5017 (2020).

56. Wallace, J. M., Smith, C. & Bretherton, C. S. Singular Value Decomposition of Wintertime Sea Surface Temperature and 500-mb Height Anomalies. *J. Clim.* **5**, 561–576 (1992).

57. Bretherton, C. S., Smith, C. & Wallace, J. M. An Intercomparison of Methods for Finding Coupled Patterns in Climate Data. *J. Clim.* **5**, 541–560 (1992).

58. Fan, T. et al. Emission or atmospheric processes? An attempt to attribute the source of large bias of aerosols in eastern China simulated by global climate models. *Atmos. Chem. Phys.* **18**, 1395–1417 (2018).

59. Fan, T. et al. Comparison of the Anthropogenic Emission Inventory for CMIP6 Models with a Country-Level Inventory over China and the Simulations of the Aerosol Properties. *Adv. Atmos. Sci.* **39**, 80–96 (2022).

60. Zeng, L. et al. Intensified modulation of winter aerosol pollution in China by El Niño with short duration. *Atmos. Chem. Phys.* **21**, 10745–10761 (2021).

61. Meehl, G. A. et al. Climate Change Projections in CESM1(CAM5) Compared to CCSM4. *J. Clim.* **26**, 6287–6308 (2013).

62. Zelinka, M. D., Andrews, T., Forster, P. M. & Taylor, K. E. Quantifying components of aerosol-cloud-radiation interactions in climate models. *J. Geophys. Res. Atmos.* **119**, 7599–7615 (2014).

63. Samset, B. H. et al. Climate Impacts From a Removal of Anthropogenic Aerosol Emissions. *Geophys. Res. Lett.* **45**, 1020–1029 (2018).

64. Lu, Z. et al. Radiative Forcing of Nitrate Aerosols From 1975 to 2010 as Simulated by MOSAIC Module in CESM2-MAM4. *J. Geophys. Res. Atmos.* **126**, e2021JD034809 (2021).

65. Hsu, N. C. et al. Enhanced Deep Blue aerosol retrieval algorithm: The second generation. *J. Geophys. Res. Atmos.* **118**, 9296–9315 (2013).

66. Hersbach, H. et al. The ERA5 global reanalysis. *Q. J. R. Meteorol. Soc.* **146**, 1999–2049 (2020).

67. Hurrell, J. W. et al. The Community Earth System Model: A Framework for Collaborative Research. *Bull. Am. Meteorol. Soc.* **94**, 1339–1360 (2013).

68. Liu, X. et al. Description and evaluation of a new four-mode version of the Modal Aerosol Module (MAM4) within version 5.3 of the Community Atmosphere Model. *Geosci. Model Dev.* **9**, 505–522 (2016).

69. Liu, X. et al. Toward a minimal representation of aerosols in climate models: description and evaluation in the Community Atmosphere Model CAM5. *Geosci. Model Dev.* **5**, 709–739 (2012).

70. Morrison, H. & Gettelman, A. A New Two-Moment Bulk Stratiform Cloud Microphysics Scheme in the Community Atmosphere Model, Version 3 (CAM3). Part I: Description and Numerical Tests. *J. Clim.* **21**, 3642–3659 (2008).

71. Gettelman, A., Morrison, H. & Ghan, S. J. A New Two-Moment Bulk Stratiform Cloud Microphysics Scheme in the Community Atmosphere Model, Version 3 (CAM3). Part II: Single-Column and Global Results. *J. Clim.* **21**, 3660–3679 (2008).

72. Iacono, M. J. et al. Radiative forcing by long-lived greenhouse gases: Calculations with the AER radiative transfer models. *J. Geophys. Res. Atmos.* **113**, D13103 (2008).

73. Wang, H. et al. Sensitivity of remote aerosol distributions to representation of cloud–aerosol interactions in a global climate model. *Geosci. Model Dev.* **6**, 765–782 (2013).

74. Wang, Z. et al. Incorrect Asian aerosols affecting the attribution and projection of regional climate change in CMIP6 models. *npj Clim. Atmos. Sci.* **4**, 1–8 (2021).

75. van Marle, M. J. E. et al. Historic global biomass burning emissions for CMIP6 (BB4CMIP) based on merging satellite observations with proxies and fire models (1750–2015). *Geosci. Model Dev.* **10**, 3329–3357 (2017).

76. Guenther, A. B. et al. The Model of Emissions of Gases and Aerosols from Nature version 2.1 (MEGAN2.1): an extended and updated framework for modeling biogenic emissions. *Geosci. Model Dev.* **5**, 1471–1492 (2012).

77. Lund, M. T. et al. Concentrations and radiative forcing of anthropogenic aerosols from 1750 to 2014 simulated with the Oslo CTM3 and CEDS emission inventory. *Geosci. Model Dev.* **11**, 4909–4931 (2018).

78. Takaya, K. & Nakamura, H. A Formulation of a Phase-Independent Wave-Activity Flux for Stationary and Migratory Quasigeostrophic Eddies on a Zonally Varying Basic Flow. *J. Atmos. Sci.* **58**, 608–627 (2001).

AUTHOR CONTRIBUTIONS

J.G. conducted the model simulations and performed the analysis. Y.Y. conceived the research and directed the analysis. All the authors discussed the results and wrote the paper.

COMPETING INTERESTS

The authors declare no competing interests.

ADDITIONAL INFORMATION

Supplementary information The online version contains supplementary material available at https://doi.org/10.1038/s41612-023-00488-y.

Correspondence and requests for materials should be addressed to Yang Yang.

Reprints and permission information is available at http://www.nature.com/reprints

Publisher's note Springer Nature remains neutral with regard to jurisdictional claims in published maps and institutional affiliations.